The Linear Absorption and Pump−Probe Spectra of Cylindrical Molecular Aggregates

Mariusz Bednarz[†,‡] and Jasper Knoester*[,‡]

Institute of Theoretical Physics, Warsaw University, Hoża Street 69, 00-681 Warsaw, Poland, and Institute for Theoretical Physics and Material Science Center, University of Groningen, Nijenborgh 4, 9747 AG Groningen, The Netherlands

Received: June 21, 2001

We study the optical response of Frenkel excitons in molecular J aggregates with a cylindrical geometry. Such aggregates have recently been prepared for a class of cyanine dyes and are akin to the rod- and ring-shaped light-harvesting systems found in certain bacteria. The linear absorption spectrum exhibits two lines with perpendicular polarization that are separated by a "ring energy scale", which is set by the circumference of the cylinder and the intermolecular transfer interaction in the circumferential direction. On the other hand, the pump−probe spectrum shows bleaching and induced absorption features that are separated by a much smaller energy scale, which is determined by an effective Pauli gap imposed by the length of the cylinder and the transfer interaction in its longitudinal direction. We show that this can be well-understood from the approximate separation of the set of two-exciton states, into classes of inter-ring and intra-ring two-exciton states. Our calculations show that the experimental linear absorption spectrum may be used to estimate the cylinder circumference, while the pump−probe spectrum yields information on the length of the cylinder or on the delocalization length of the excitons in its longitudinal direction. We apply this method to cylindrical aggregates of cyanine dyes.

I. Introduction

The optical properties of Frenkel excitons in molecular aggregates of various compositions and geometries have aroused much attention during the past decade. Best known are the self-assembled linear J aggregates of cyanine dyes.[1−3] Using the Langmuir−Blodgett technique, the same dyes may be used to form two-dimensional aggregates.[4,5] Yet other classes of aggregates are the discostic H aggregates formed by, e.g, triarylpyrylium salts[6] or hexa-alkyloxytriphenylenes,[7] and pinwheel nanoaggregates of conjugated oligomers.[8] In addition, nature has provided us with very regular aggregate structures. For example, ring-shaped assemblies of chlorophyll molecules play an important role in the photosynthetic antenna systems of purple bacteria.[9,10] The efficient energy transport properties of these ring aggregates have recently attracted much attention;[11] understanding these properties is considered an important step toward further development of artificial antenna systems. Other natural antenna complexes (those of green bacteria) have been found to have a rod-shape (cylindrical) structure.[12−14]

While the exciton dynamics on cylindrical antennae seems to be studied in less detail than for the ring-shaped ones, the cylindrical geometry does offer interesting new possibilities for fast and efficient transport, as it combines the ring-shaped geometry with a second propagation dimension. In principle, this makes the excitons less sensitive to the localizing effects of disorder. Interestingly, during the past few years, cylindrical aggregates have also been prepared through self-aggregation of cyanine dyes with various substituents.[15,16] Optical absorption and CD measurements, as well as cryo-TEM pictures indicate the existence of J aggregates (red-shifted optical absorption relative to the monomer) with a cylindrical shape and a certain helicity.[15−17] The individual cylinders have a diameter of the order of 10 nm and a length of several micrometers; they may occur singly or in ropes of several cylinders twisted around each other. The microscopic structure of the individual cylinders is unknown, although in the case of longer substituents a micellar structure has been suggested.[15] The red-shifted absorption band indicates that the dominant excitation transfer interaction is negative (head-to-tail-type arrangement), while the CD spectrum indicates that the molecular dipoles have components both along the cylinder axis and perpendicular to it.

In this paper, we consider the theory of the linear absorption and pump−probe spectra of cylindrical aggregates that consist of a stack of interacting rings. As not much theory has been developed for these aggregate geometries, we will restrict ourselves to the simple case of homogeneous aggregates. As noted above already, the two-dimensional character of these aggregates helps to overcome effects of disorder, implying that a zero-disorder assumption may already grasp the essential features. This even holds for one-dimensional aggregates, provided that we replace the aggregate length by the exciton localization length.[18,19]

In particular, for one-dimensional aggregates, the frequency separation (Pauli exclusion gap) between the one-exciton bleaching peak and the one- to two-exciton induced absorption contributions in the pump−probe spectrum[20−23] is a measure for the aggregate size or, in the case of disordered aggregates, the exciton delocalization length.[24−26] As we will demonstrate in this paper, the optical spectra of cylindrical aggregates may reveal similar information. In particular, we will show that under certain circumstances, the linear absorption spectrum may be

* Corresponding author. Fax: +31-50 3634947. E-mail: knoester@phys.rug.nl.
† Warsaw University.
‡ University of Groningen.

10.1021/jp012371n CCC: $20.00
Published on Web 11/30/2001

used to obtain information on the circumference of the cylinder, while the pump−probe spectrum contains information on the length of the cylinder or on the delocalization length in its longitudinal direction. The fact that both spectra reveal different length scales is a consequence of the particular optical selection rules in cylindrical aggregates and of the fact that the two-exciton states on the cylinder may, to a very good approximation, be distinguished into those that have a ring-like character (intra-ring two-exciton states) and those that have a longitudinal character (inter-ring two-exciton states). In general, both classes have different Pauli exclusion gaps, reflecting the difference in longitudinal and circumferential length scales.

The outline of this paper is as follows. In section II, we present the model and discuss the main features of the linear absorption spectrum. Connection to experiment is made. In section III, we present the general expression for the pump−probe spectrum and simplified expressions for the case of nearest-neighbor interactions. A systematic study of the results of these expressions is presented in section IV, where we plot the pump−probe spectrum for various choices of intermolecular transfer interactions, line widths, and cylinder sizes. Particular attention is paid to the evolution of the spectrum from a single-ring one, obtained in the limit of vanishing interactions in the longitudinal direction of the cylinder, to the full cylinder spectrum. This reveals a dramatic change of energy scale from a "ring scale" to a "longitudinal scale", resulting from the different Pauli gaps mentioned above. We explain the physics behind our results in section V, by introducing the intra-ring and inter-ring two-exciton states. Finally, in section VI, we connect to recent experiments and we conclude.

II. Model and Linear Absorption

Our aggregate model consists of a rectangular lattice folded onto a cylinder and occupied by one dye molecule per unit cell (Figure 1). The molecular positions may thus be denoted by a two-dimensional vector $\mathbf{n} = (n_1,n_2)$, where $n_1 = 1, 2, ..., N_1$ and $n_2 = 1, 2, ..., N_2$. Here n_1 labels the position along the longitudinal direction of the cylinder, while n_2 labels the position along the circumference. N_1, the length of the cylinder, is large and may be taken infinite for most of the cases that we will consider. This justifies taking periodic boundary conditions in the longitudinal direction. By contrast, N_2 is finite (on the order of ten); in this direction, periodic boundary conditions are rigorous, due to the cylindrical geometry.

To describe the optical excitations of the aggregate, we will adhere to the Frenkel exciton model and assume that the molecules may be considered two-level chromophores. The corresponding Hamiltonian reads:[27,28]

$$H = \epsilon \sum_{\mathbf{n}} b_{\mathbf{n}}^{\dagger} b_{\mathbf{n}} + \sum_{\mathbf{n}} \sum_{\mathbf{m}} J(\mathbf{m}) b_{\mathbf{n}+\mathbf{m}}^{\dagger} b_{\mathbf{n}} \qquad (1)$$

Here, $b_{\mathbf{n}}^{\dagger}$ ($b_{\mathbf{n}}$) denotes the Pauli creation (annihilation) operator for an excitation on molecule **n**. The summations over **n** and **m** both extend over the entire cylinder surface, with the above-noted periodic boundary conditions in both lattice directions implied. Finally, ϵ is the molecular excitation energy, while $J(\mathbf{m})$ is the excitation transfer interaction between two molecules that are separated by the vector **m** on the underlying lattice. Obviously, the above Hamiltonian assumes translational invariance (absence of disorder), as was already argued in the Introduction. We also note that H neglects non-Heitler−London effects.[29,30]

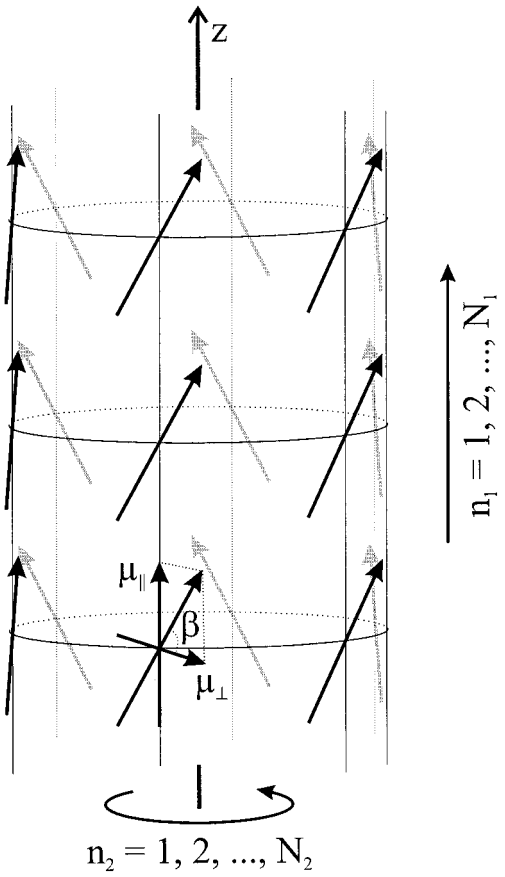

Figure 1. Schematic picture of the cylindrical aggregate. Two-level molecules occupy a rectangular lattice that has been folded on the cylinder, with one lattice direction parallel to the cylinder axis. Each ring contains N_2 molecules, while the length of the cylinder is N_1 lattice constants. The arrows indicate the transition dipoles of the molecules. These dipoles have equal z components ($\mu_{\|}$) for all molecules, while the component perpendicular to the z axis is equal in magnitude ($\mu_{\perp}$) for all molecules and rotates around the cylinder with the molecular position. The angle between the dipoles and the xy plane is denoted β.

As the typical transfer interaction is small compared to ϵ, the ground state $|g\rangle$ of the above Hamiltonian is the state with all molecules in their respective ground states. Due to the translational symmetry, the one-exciton excitations are immediately found to be

$$|\mathbf{q}\rangle = N^{-1/2} \sum_{\mathbf{n}} e^{i\mathbf{q}\cdot\mathbf{n}} b_{\mathbf{n}}^{\dagger} |g\rangle \qquad (2)$$

where $N = N_1 N_2$, the total number of molecules. The label **q** denotes the wave vector (momentum) of the Bloch state, which has components $q_i = 2\pi l_i/N_i$ ($i = 1, 2$), where $l_i = 0, 1, ..., N_i - 1$. The energy of the state $|\mathbf{q}\rangle$ is denoted $E_{\mathbf{q}}$, given by

$$E_{\mathbf{q}} = \epsilon + \sum_{\mathbf{m}} J(\mathbf{m}) \cos(\mathbf{q}\cdot\mathbf{m}) \qquad (3)$$

The next higher manifold of states are the two-exciton ones, in which the molecules on the cylinder share two excitation quanta. These states cannot as readily be written down, due to the kinematic interaction imposed by the Pauli exclusion of double excitation of each molecule. We will come back to these states when dealing with the pump−probe spectrum in sections III and V. In the remainder of this section, we will focus on the linear absorption spectrum, for which it suffices to consider the transitions from the ground state to the one-exciton manifold.

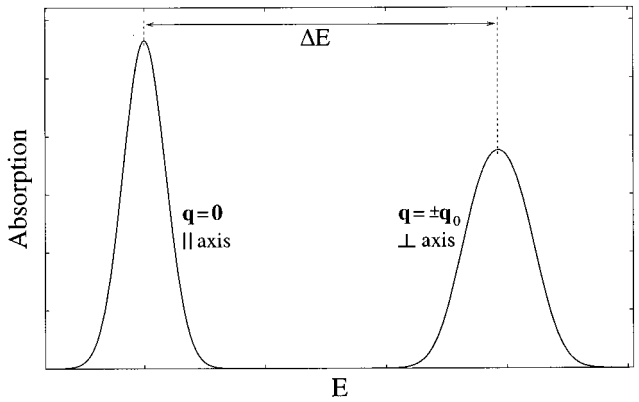

Figure 2. Schematic representation of the linear absorption spectrum of a cylindrical aggregate consisting of a stack of rings. We have assumed that ΔE, as defined in eq 8, is positive, as is appropriate for J aggregates. Three Bloch states are visible in absorption, one of which ($\mathbf{q} = \mathbf{0}$) is polarized parallel to the cylinder axis, while the other two ($\mathbf{q} = \pm\mathbf{q}_0$) are degenerate and are polarized perpendicular to the axis.

At this point, we also need to fix the molecular transition dipoles. Again, we will assume perfect translational symmetry, implying that all molecules have dipoles that are equal in magnitude (μ) and that have equal orientations relative to the local orientation of the cylinder surface at the position of the molecule. Thus, the components of the dipoles in the direction of the cylinder axis are equal for all molecules: $\mu_{||} = \mu \sin \beta$, with β the angle between the molecular dipoles and the plane perpendicular to the cylinder axis (see Figure 1); the components perpendicular to the axis have magnitude $\mu_\perp = \mu \cos \beta$ and rotate around the axis when moving around the rings that make up the cylinder. For explicitness, we will define the z direction along the axis of the cylinder, the x direction along the projection of the dipoles of the molecules with coordinates (n_1, $n_2 = N_2$) on a plane perpendicular to the cylinder axis, and the y direction in the same plane, perpendicular to the x direction. Then the transition dipole of the molecule on site $\mathbf{n}$ reads:

$$\vec{\mu}_{\mathbf{n}} = (\mu_\perp \cos(\mathbf{n}\cdot\mathbf{q}_0), \mu_\perp \sin(\mathbf{n}\cdot\mathbf{q}_0), \mu_{||}) \qquad (4)$$

where $\mathbf{q}_0 = (0, q_0)$ with $q_0 = 2\pi/N_2$. (Arrows over symbols denote three-dimensional vectors in real space, as opposed to the bold symbols, which refer to the two-dimensional cylinder surface or its reciprocal space).

We now turn to the matrix elements $\vec{\mu}_{\mathbf{q}} \equiv \langle \mathbf{q}|\hat{\vec{\mu}}|g\rangle$ of the cylinder's total dipole operator $\hat{\vec{\mu}} \equiv \sum_{\mathbf{n}} \vec{\mu}_{\mathbf{n}} (b_{\mathbf{n}}^\dagger + b_{\mathbf{n}})$ between the ground state and the one-exciton states. The three components of this transition dipole read:

$$\mu_{\mathbf{q},x} = \frac{\mu_\perp}{2} \sqrt{N} (\delta_{\mathbf{q},\mathbf{q}_0} + \delta_{\mathbf{q},-\mathbf{q}_0}) \qquad (5)$$

$$\mu_{\mathbf{q},y} = \frac{\mu_\perp}{2i} \sqrt{N} (\delta_{\mathbf{q},\mathbf{q}_0} - \delta_{\mathbf{q},-\mathbf{q}_0}) \qquad (6)$$

$$\mu_{\mathbf{q},z} = \mu_{||} \sqrt{N} \delta_{\mathbf{q},\mathbf{0}} \qquad (7)$$

Thus, only three states are dipole allowed (and in fact superradiant), namely, $|\mathbf{q}\rangle = |\mathbf{0}\rangle, |\pm\mathbf{q}_0\rangle$. We note that the latter two are degenerate (cf. eq 3) and have polarization perpendicular to the cylinder axis, while the first transition is polarized parallel to the cylinder axis. As a result, the linear absorption spectrum is dominated by two peaks (Figure 2), with mutually perpendicular polarization and separated by the energy

$$\Delta E = E_{\pm\mathbf{q}_0} - E_{\mathbf{0}} = \sum_{m_2 \neq 0} j(m_2)(\cos(q_0 m_2) - 1) \qquad (8)$$

with $j(m_2) = \sum_{m_1} J(\mathbf{m})$, which is the total excitation transfer interaction between a given molecule and all the molecules on the line parallel to the cylinder axis and shifted relative to the given molecule by m_2 lattice units in the circumferential direction of the cylinder.

Measurements on the cylindrical aggregates of the cyanine dye TDBC/C8O3 (5,5′,6,6′-tetrachloro-1,1′-dioctyl-3,3′di(3-carboxypropyl) -benzimidacarbocyanine) in a stretched polymer film indeed confirm the existence of two absorption lines of perpendicular polarization.[17] We point out that, unlike the explanation that is common for organic molecular crystals and aggregates, the occurrence of two lines of perpendicular polarization in our case does not relate to a Davydov splitting,[27,28] but is purely a result of the global (cylindrical) geometry of the aggregate with one molecule per unit cell.

As is clear from eq 8, the splitting ΔE allows one to determine the cylinder circumference N_2, provided that one has detailed information on the spatial dependence of the transfer interactions. Generally, such detailed information is lacking. However, in the case that the interactions between molecules on different rings are very weak compared to the ones within a single ring and the latter ones are taken in nearest-neighbor approximation ($-J_2$), we have $\Delta E = -2J_2(\cos(2\pi/N_2) - 1)$. This suffices to determine N_2, as $-2J_2$ can then be measured from the shift of the absorption peak with parallel polarization ($\mathbf{q} = \mathbf{0}$ exciton) relative to the molecular transition frequency ϵ. Within this assumption, the cylinder circumference for aggregates of the dye TDBC/C8O3 was determined to be 7 or 8 molecules in ref 17, which is in reasonable agreement with the information on the cylinder diameter as derived from cryo-TEM and filtration.[16,17] We also note that the ratio of the areas under both absorption lines, $A_{\pm\mathbf{q}_0}/A_{\mathbf{0}} = (\mu_\perp/\mu_{||})^2 = \tan^2 \beta$, allows one to measure the angle β of the molecular orientation. To end this section, we mention that weak disorder broadens both absorption lines and may, under special circumstances, lead to a fine-structure in the $\pm\mathbf{q}_0$ line.[31]

III. Pump−Probe Spectrum: General Theory

We now turn to the pump−probe (or transient absorption) spectrum for cylindrical aggregates. For weak-intensity pulses, the pump−probe experiment is a third-order technique, which, neglecting coherent "artifacts",[32] may be considered a sequence of two linear absorption experiments. The general features of this spectrum for Frenkel exciton systems are well-known and can be separated into negative contributions (ground-state bleaching and stimulated emission of the one-exciton states excited by the pump pulse) and positive ones (induced absorption from the pumped one-exciton states to the two-exciton states).[20−23] Thus, in principle, the pump−probe spectrum involves calculating the two-exciton states. Even if we neglect dynamic exciton−exciton interactions (as we did in the Hamiltonian eq 1), calculating these states is not straightforward, due to the Pauli exclusion of doubly exciting a single molecule. Using the hard-core boson approach, however, it suffices to calculate the one-exciton energies and transition dipoles in order to calculate the pump−probe spectrum.[33,34] For our case of translational symmetry (with periodic boundary conditions) and one molecule per unit cell, the general result is given by

$$\Delta I(E) = \mathrm{Im}\frac{2}{\pi}\sum_{\mathbf{q},\mathbf{q}'}\frac{f(\mathbf{q})|\vec{\mu}_{\mathbf{q}'}\cdot\vec{e}\,|^2}{(E - E_{\mathbf{q}'} + i\eta)^2}[G(E;\mathbf{q},\mathbf{q}')]^{-1} \quad (9)$$

with

$$G(E;\mathbf{q},\mathbf{q}') = \sum_{\mathbf{k}}\frac{1}{E + E_{\mathbf{q}} - E_{(\mathbf{q}+\mathbf{q}')/2+\mathbf{k}} - E_{(\mathbf{q}+\mathbf{q}')/2-\mathbf{k}} + i\eta} \quad (10)$$

These expressions represent a straightforward generalization of eq 43 in ref 34 in the sense that we now allow the aggregate to reside in a superposition of exciton populations just before the probe pulse arrives. In particular, the population of the one-exciton state $\mathbf{q}$ is denoted $f(\mathbf{q})$. This population may be created by the pump pulse or in a relaxation process taking place after the initial excitation. Furthermore, E denotes the photon energy in the probe pulse, η is the homogeneous line width, $E_{\mathbf{q}}$ is the one-exciton dispersion (eq 3), $\vec{\mu}_{\mathbf{q}'}$ indicates the transition dipole from the ground state to the one-exciton state $|\mathbf{q}'\rangle$ (cf. eqs 5−7), and $\vec{e}$ is the three-dimensional polarization vector of the electric field of the probe pulse. The components of the one-exciton wave vectors $\mathbf{q}$ and $\mathbf{q}'$ are quantized as given below eq 2, while the components of $\mathbf{k}$ take the values $k_i = 2\pi l_{ki}/N_i$, where $l_{ki} = 0, 1, ..., N_i - 1$ if $(q_i + q_i')N_i/(2\pi)$ is even and $l_{ki} = {}^1/_2, {}^3/_2, ..., N_i - {}^1/_2$ otherwise.

The physical meaning of eqs 9 and 10 is as follows. One first thinks of the excitons as bosons. The initial condition (created by the pump pulse) is that one boson (one-exciton) with momentum $\mathbf{q}$ and energy $E_{\mathbf{q}}$ is present with probability $f(\mathbf{q})$. The probe pulse of energy E creates a second boson, with momentum $\mathbf{q}'$. The probability of this process is described by the oscillator strength of this state and the resonance factor in eq 9. As a result of the Pauli exclusion of the double excitation of a single molecule, however, the bosons are subject to a mutual repulsive hard-core potential. This potential scatters the pair of bosons into other pairs, conserving its center of mass momentum $\mathbf{q} + \mathbf{q}'$, but allowing for a change in the relative momentum $\mathbf{k}$. The amplitude of this scattering process is represented by $G(E;\mathbf{q},\mathbf{q}')$.

For general transfer interactions $J(\mathbf{m})$, further steps cannot be taken analytically, but involve numerical evaluation of eq 9 using, e.g, the detailed calculation of (extended) dipole−dipole transfer interactions for the geometry considered. While such numerical implementation is quite straightforward in principle, we prefer to focus here on generic effects, which may already be obtained from simple model interactions. Specifically, in what follows, we will consider nearest-neighbor interactions: $J(\mathbf{m}) = -J_1(\delta_{m_1,1} + \delta_{m_1,-1})\delta_{m_2,0} - J_2\delta_{m_1,0}(\delta_{m_2,1} + \delta_{m_2,-1})$, i.e., the nearest-neighbor interaction along the longitudinal direction (between adjoining rings) of the cylinder has value $-J_1$, while the one along the circumferential direction (along a ring) has value $-J_2$. Then the one-exciton energies read

$$E_{\mathbf{q}} = \epsilon - 2J_1\cos q_1 - 2J_2\cos q_2 \quad (11)$$

and we have

$$G(E;\mathbf{q},\mathbf{q}') = \sum_{\mathbf{k}}\frac{1}{E - \epsilon - J_1 h(q_1,q_1',k_1) - J_2 h(q_2,q_2',k_2) + i\eta} \quad (12)$$

with $h(q_i,q_i',k_i) = 2\cos q_i - 4\cos((q_i + q_i')/2)\cos k_i$.

The numerical effort involved in calculating $G(E;\mathbf{q},\mathbf{q}')$ may be reduced because the summation over k_1 in eq 12 can be performed analytically. This leaves us with a summation over only N_2 terms. We will not give the explicit expressions here, as the method of summation is well-documented[35,36] and has been applied to a similar situation (a monolayer) in ref 34.

IV. Results

In almost all examples considered in this paper, we will assume that the cylinder resides in the $\mathbf{q} = \mathbf{0}$ one-exciton state at the moment that the probe arrives, i.e., $f(\mathbf{q}) = \delta_{\mathbf{q},\mathbf{0}}$. This is the case (i) if one pumps in the $\mathbf{q} = \mathbf{0}$ linear absorption band (see Figure 2) and applies pump−probe delay times that are short compared to any possible relaxation times within the exciton band or (ii) if one uses long delay times, provided that the temperature is small enough and the $\mathbf{q} = \mathbf{0}$ one-exciton state lies at the bottom of the one-exciton band. The latter occurs if both J_1 and J_2 are positive, which we will refer to as the "JJ" aggregate, i.e., J aggregate nature (negative transfer interactions) in both lattice directions. Situation (i) is independent of whether the $\mathbf{q} = \mathbf{0}$ state lies at the bottom of the one-exciton band.

For definiteness, we will first assume that, indeed, we are dealing with a JJ aggregate. For nearest-neighbor transfer interactions $-J_1$ and $-J_2$ of point-dipole origin, this is the case if the molecular dipoles are oriented tangential to the surface of the cylinder and make an angle β with one of the lattice directions given by $35.3° < \beta < 54.7°$. Including long-range interactions and (or) the extended dipole nature may change those boundaries (see section VI).

Figure 3 shows a sequence of pump−probe spectra calculated (using the expressions derived in section III) for JJ cylinders with $f(\mathbf{q}) = \delta_{\mathbf{q},\mathbf{0}}$, $N_1 = 100$, $N_2 = 10$, $\eta/J_2 = 0.01$, and various values of J_1/J_2. Here the value for N_1 has been chosen considerably larger than the coherence length imposed by the line width η

$$N_{\mathrm{coh}} \equiv (2\pi^2 J_1/\eta)^{1/2} \quad (13)$$

above which the spectrum has reached its infinite N_1 limit.[37] N_2 has been chosen as a value that seems typical for the cylinders observed in ref 17. The solid curves represent the spectrum for a probe polarized parallel to the cylinder axis, while the dashed curves refer to a probe perpendicular to the axis (for an isotropic distribution of axis orientations, as in solution, the measured spectrum will be a linear combination of the two).

Figure 3a, with $J_1 = 0$, represents the single-ring spectrum. In parallel polarization, this exhibits a negative bleaching and stimulated emission feature at $E_{\mathbf{q}=\mathbf{0}} = \epsilon - 2J_2$ and a positive induced absorption peak that is blue shifted relative to the bleaching peak by an amount

$$\Delta_\perp = 4J_2(1 - \cos(\pi/N_2)) \approx 2\pi^2 J_2/N_2^2 \quad (14)$$

This detuning represents the "Pauli exclusion gap" for the two-exciton states in a single ring and follows from the analytical solution of these states (cf. section V).[38−40] The parameter $\Delta_\perp$ defines a typical frequency scale for the pump−probe spectrum of the ring. This scale is determined by the interaction J_2 and the ring size N_2 and is of the same order of magnitude as the detuning ΔE between the two peaks in the linear absorption spectrum (cf. section II). In perpendicular polarization, we see similar features, which are blue shifted relative to the parallel case. The bleaching peak (no stimulated emission) occurs at $E_{\mathbf{q}=\pm\mathbf{q}_0}$, the energy of the only dipole allowed one-exciton states in this polarization. The induced absorption

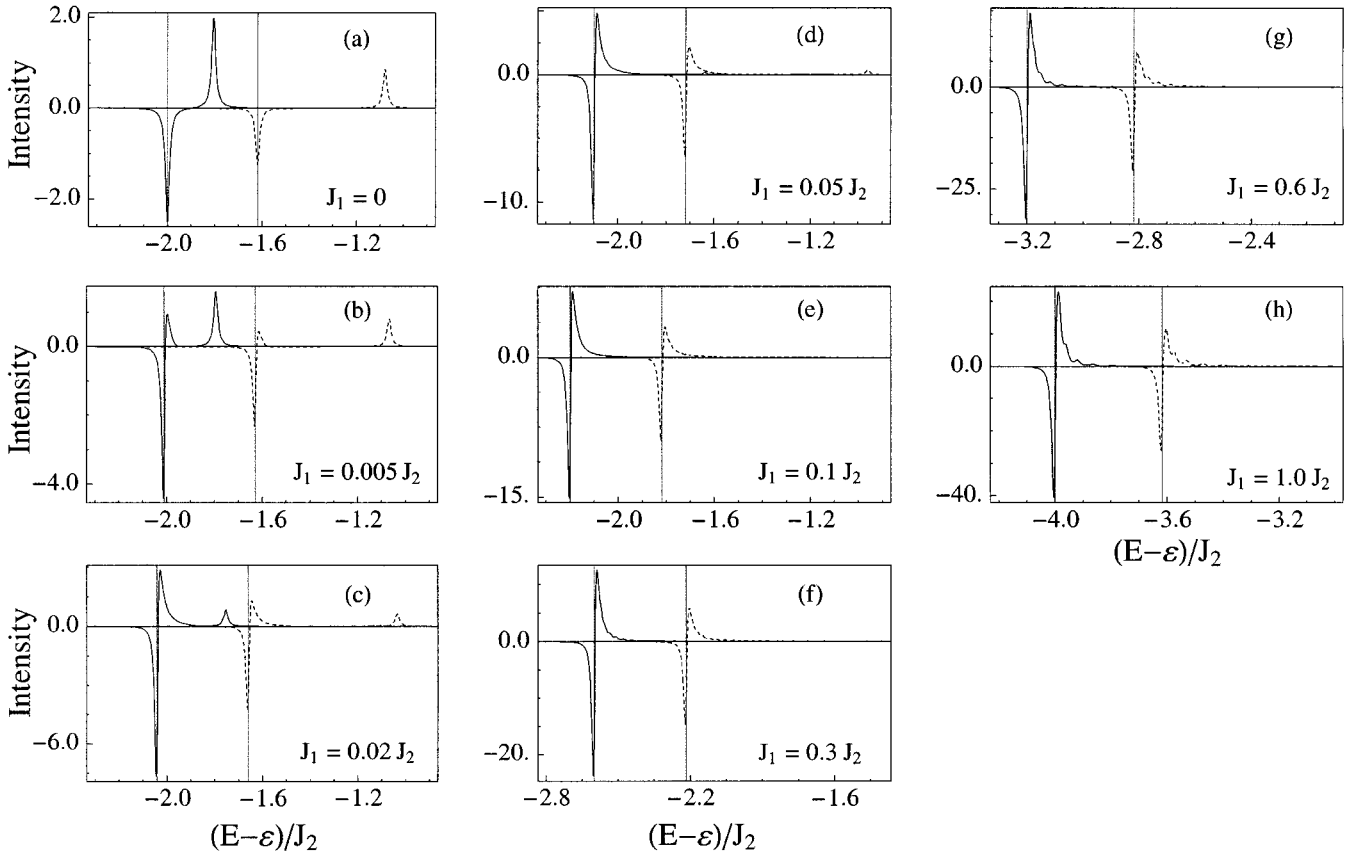

Figure 3. Pump-probe spectrum for a cylindrical JJ aggregate of length $N_1 = 100$ and circumference $N_2 = 10$ molecules for $J_1/J_2 = 0$ (a), 0.005 (b), 0.02 (c), 0.05 (d), 0.1 (e), 0.3 (f), 0.6 (g), and 1.0 (h). In all cases, the cylinder resides in the $|\mathbf{q} = \mathbf{0}\rangle$ one-exciton state at the moment that the probe pulse arrives. The solid curves display the spectra if the probe is polarized parallel to the cylinder axis (intensity in units of $8\mu_{||}^2/(\pi\eta)$), while dashed curves represent the case of perpendicular polarization (intensity in units of $\mu_\perp{}^2/(\pi\eta)$). The line width η has been taken $0.01J_2$ for all panels. The light vertical lines represent the positions of the two linear absorption peaks in parallel polarization ($E_{\mathbf{q}=\mathbf{0}}$) and perpendicular polarization ($E_{\mathbf{q}=\pm\mathbf{q}_0}$), respectively.

in this polarization is again separated from the corresponding bleaching peak by an amount of the order $\Delta_\perp$ (more precisely $\sim 3\Delta_\perp$).

Figure 3b shows the same spectra for $J_1 = 0.005J_2$. We note that this weak interaction between the rings already gives an appreciable change in the pump−probe spectrum for both probe polarizations. We still observe the bleaching peaks; they are slightly red-shifted compared to Figure 3a, as a consequence of the red-shift of the exciton band edge $E_{\mathbf{q}=\mathbf{0}}$ for $J_1 > 0$. We also still see the ring-induced absorption peaks, which are slightly blue shifted compared to the $J_1 = 0$ situation and which have lost some intensity. Most interestingly, however, we observe that in both polarizations, new induced absorption contributions have arisen slightly blue-shifted relative to the corresponding bleaching peak. The frequency scale between the bleaching and this new induced absorption peak is (in both polarizations) considerably smaller than $\Delta_\perp$ and, for the current value of N_1, is set by the line width η (see section V for more detail). We also observe that the maximum intensity of the bleaching features has grown relative to Figure 3a.

The observed trends continue upon further increasing J_1/J_2, as can be seen in panels c−e of Figure 3, which represent the cases $J_1/J_2 = 0.02$, 0.05, and 0.1, respectively. In the latter case, the induced absorption peaks associated with the ring have become invisible relative to the large bleaching and induced absorption features at $E_{\mathbf{q}=\mathbf{0}} = \epsilon - 2J_2 - 2J_1$ (parallel polarization) and $E_{\mathbf{q}=\pm\mathbf{q}_0} \approx \epsilon - 2J_2 - 2J_1 + 2\Delta_\perp$ (perpendicular polarization). These remaining features in both polarizations have now obtained the familiar dispersive shape that characterizes the pump−probe spectra of one-dimensional J aggregates.[20−23] If we now further increase J_1/J_2 (Figure 3f−h), these dispersive features obtain a fine structure, that starts to compete with the line broadening η. This fine structure is resolved if we lower η, just as is the case for one-dimensional J aggregates.[37,41] We show this in Figure 4, where we focus on a small energy region close to the dispersive feature for the case $\eta = 10^{-4}J_2$, with three different combinations of J_1/J_2 and N_1 (parallel polarization only). In all cases, the induced absorption feature of Figure 3f−h splits up in several well-separated contributions, of which in panels b and c of Figure 4 only the dominant contribution is seen. This dominant positive peak is blue shifted relative to the bleaching peak by an amount that agrees well with

$$\Delta_{||} = 4J_1(1 - \cos(\pi/N_1)) \approx 2\pi^2 J_1/N_1^2 \qquad (15)$$

which represents an effective Pauli exclusion gap in a ring of two-level molecules with length N_1 and intermolecular interactions J_1.

In summary, for the JJ aggregate, we observe a quite spectacular change of the pump−probe spectrum of the cylinder when increasing the inter-ring interaction J_1 from zero to J_2. In particular, we see a rapid change of the dominant frequency scale in the spectrum from the single-ring scale $\Delta_\perp$ to a much smaller scale that is determined by either the line broadening η

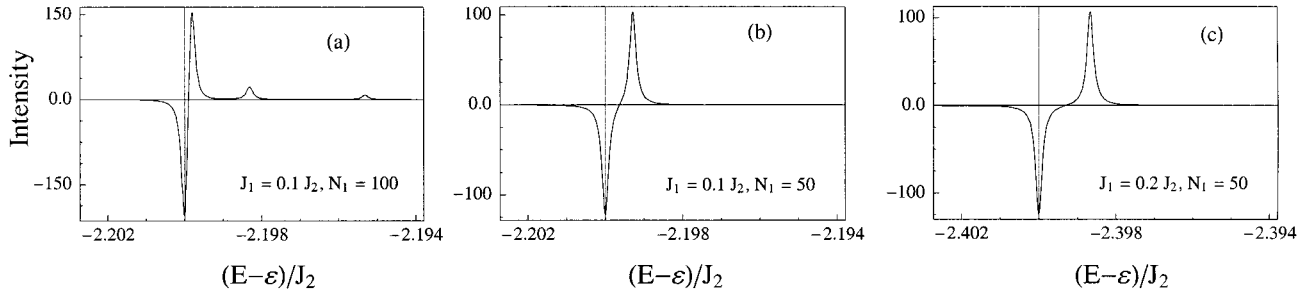

Figure 4. Same as Figure 3, but now we have chosen a smaller line width, $\eta = 10^{-4}J_2$, and we only display the spectrum for parallel probe polarization (the perpendicular spectrum occurs outside the current frequency scale). The cylinder circumference is $N_2 = 10$ molecules for all cases, while the other parameters are $N_1 = 100$ and $J_1/J_2 = 0.1$ (a), $N_1 = 50$ and $J_1/J_2 = 0.1$ (b), and $N_1 = 50$ and $J_1/J_2 = 0.2$ (c).

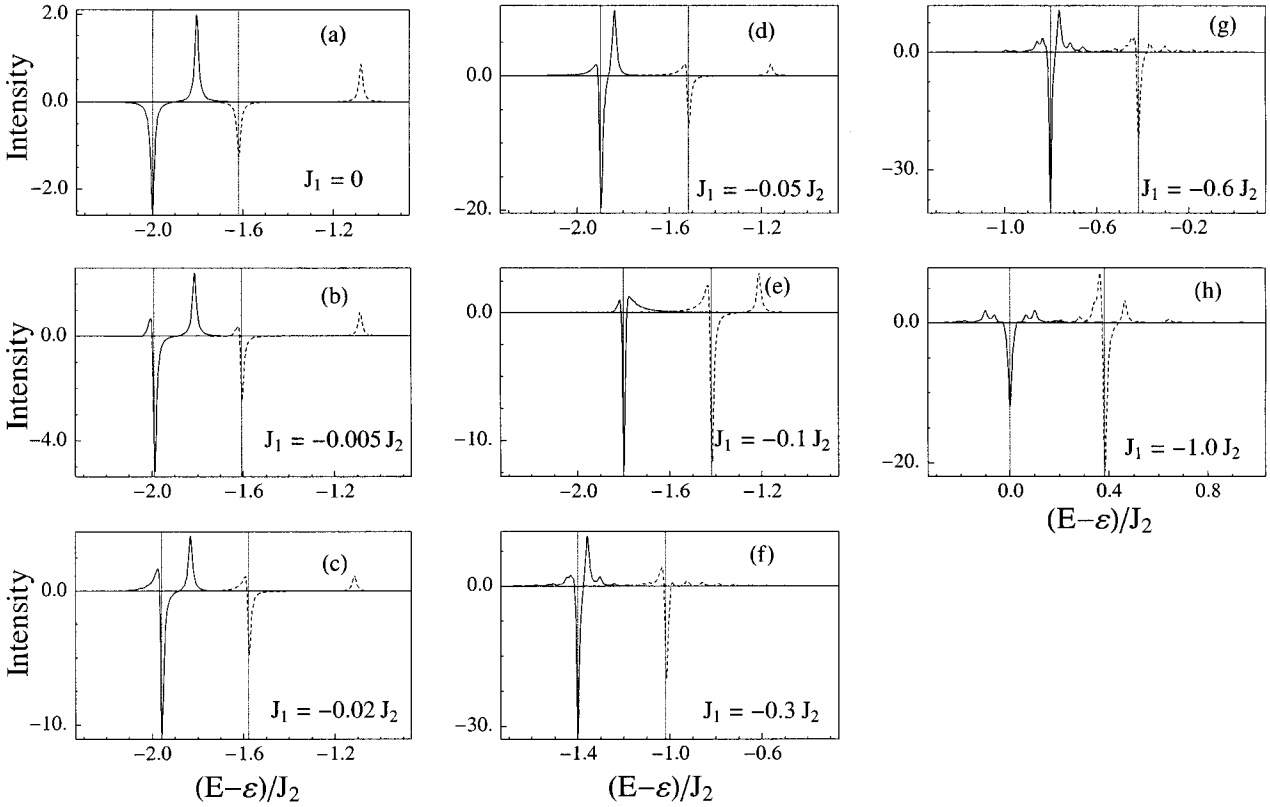

Figure 5. Same as Figure 3, but now for the HJ aggregate, with $J_1/J_2 = 0$ (a), -0.005 (b), -0.02 (c), -0.05 (d), -0.1(e), -0.3 (f), -0.6 (g), and -1.0 (h). All other parameters as those in Figure 3.

or the longitudinal scale $\Delta_{||}$. We will come back to the physical explanation of these changes in section V.

We next consider the results for the HJ aggregate, which has positive transfer interactions in the longitudinal direction (i.e., $J_1 < 0$) and negative ones in the ring direction ($J_2 > 0$). This situation typically occurs if the molecular dipoles make small angles with the plane of the ring. It should be realized that now the $\mathbf{q} = \mathbf{0}$ one-exciton state no longer lies at the bottom of the one-exciton band so that only under condition (i) discussed in the beginning of this section, the cylinder will reside in this state at the moment that the probe pulse arrives.

Figure 5 shows a series of spectra for the same parameters as those in Figure 3, except that the sign of J_1 has been reversed. For ease of comparison, we have repeated the $J_1 = 0$ limit as Figure 5a. For weak negative J_1, the phenomena observed are very similar to those for weak positive J_1. In Figure 5b, we see that for $J_1/J_2 = -0.005$, like for the case $J_1/J_2 = +0.005$, the spectrum (for both polarizations) acquires an extra induced-absorption peak, but now on the low-energy side of the bleaching peak. This is not surprising, as we have seen above that this extra induced absorption seems to be related to an effective ring of length N_1 and with interaction J_1; for negative J_1, the dispersive pump−probe feature should then become H-aggregate-like (induced absorption red-shifted relative to the bleaching peak). When we look in more detail, we see that other differences with the case $J_1/J_2 = +0.005$ are that the bleaching is slightly blue-shifted, while the ring-induced absorption peaks obtain a slight red-shift (i.e., bleaching and ring induced absorption move closer together) and slightly grow in intensity. These small differences with the positive J_1 case are the precursor of much bigger differences when we further increase $|J_1|$, as is seen in Figure 5c−h. The fact that the ring peak moves closer to the bleaching region causes interference between all main features and gives rise to a less monotonic evolution of the spectrum toward a more complicated shape than for positive J_1. In particular, we see strong induced absorption features arising on both sides of the bleaching peak. This phenomenon, which arises from the fact that the $\mathbf{q} = \mathbf{0}$ state does not lie at the bottom of the one-exciton band, was also observed for the calculated spectrum of an HJ monolayer.[34]

V. Interpretation of the Results

We now turn to the physical explanation of the phenomena observed in section IV. As we will see, this can be explained from the approximate separation of the two-exciton states on the cylinder into those with a perpendicular character (intra-ring states) and those with a more longitudinal character (inter-ring states). It will appear crucial for the observed phenomena that both classes have different Pauli gaps ($\Delta_\perp$ and $\Delta_\parallel$, respectively) and that the intra-ring states are at best superradiant in the circumference N_2 of the cylinder, while the dominant inter-ring states may be superradiant in the total number of molecules (N_1N_2) in the cylinder. Our explanation will be summarized in a pictorial way in Figure 6 below.

A. Intra-Ring and Inter-Ring Two-Exciton States. We define the intra-ring two-exciton states as those states where the two excitations are located on the same ring of the cylinder. For their orthonormal basis, we will use

$$|\mathbf{K},k_2\rangle = \frac{1}{N}\sum_{\mathbf{n},\mathbf{m}} \exp\left(i\mathbf{K}\cdot\frac{\mathbf{n}+\mathbf{m}}{2}\right) f(\mathbf{n}-\mathbf{m}) b_{\mathbf{n}}^{\dagger} b_{\mathbf{m}}^{\dagger}|g\rangle \quad (16)$$

with

$$f(\mathbf{n}-\mathbf{m}) = \delta_{n_1,m_1}\sqrt{N_1}\,\sin|k_2\frac{n_2-m_2}{2}| \quad (17)$$

Here, $\mathbf{K} = (K_1,K_2)$ is the center-of-mass (COM) momentum of the two excitations on the cylinder, which is quantized according to $K_i = 2\pi l_i/N_i$, with $l_i = 0, 1, ..., N_i - 1$. The relative momentum k_2 is only one-dimensional, as both excitations are forced to reside on the same ring ($n_1 = m_1$) and is quantized according to $k_2 = 2\pi l_2'/N_2$, with $l_2' = 1, 3, ..., N_2 - 1$ if l_2 is even and $l_2' = 2, 4, ..., N_2 - 2$ if l_2 is odd (the two upper boundaries for l_2' hold for N_2 even; if N_2 is odd, they should be interchanged). As follows from the theory of two-exciton states on a single ring,[38-40] in the absence of inter-ring interactions the above states are eigenstates of the total Hamiltonian eq 1, with energy given by

$$E_{\text{intra}}(\mathbf{K},k_2) = 2\epsilon - 4J_2\cos(K_2/2)\cos(k_2/2) \quad (18)$$

The second class of two-exciton states contains those states, where the two excitations are located on different rings (inter-ring states). We distinguish two types of different symmetry. The first type (the "+" states) take the form

$$|\mathbf{K},\mathbf{k}\rangle_+ = \frac{1}{N}\sum_{\mathbf{n},\mathbf{m}} \exp\left(i\mathbf{K}\cdot\frac{\mathbf{n}+\mathbf{m}}{2}\right) f_+(\mathbf{n}-\mathbf{m}) b_{\mathbf{n}}^{\dagger} b_{\mathbf{m}}^{\dagger}|g\rangle \quad (19)$$

with

$$f_+(\mathbf{n}-\mathbf{m}) = c(k_2)\,\sin|k_1\frac{n_1-m_1}{2}|\,\cos\left(k_2\frac{n_2-m_2}{2}\right) \quad (20)$$

Here, $\mathbf{K}$ and $\mathbf{k} = (k_1,k_2)$ are the COM and the relative momentum, respectively. The former is quantized as above, while the quantization of the latter is as follows: Its first component takes the values $k_1 = 2\pi l_1'/N_1$, with $l_1' = 1, 3, ..., N_1 - 1$ if l_1 is even and $l_1' = 2, 4, ..., N_1 - 2$ if l_1 is odd (upper boundaries interchanged if N_1 is odd). On the other hand, $k_2 = 2\pi l_2'$, with $l_2' = 0, 2, 4, ..., N_2$ if l_2 is even and $l_2' = 1, 3, ..., N_2 - 1$ if l_2 is odd (upper boundaries interchanged if N_2 is odd). The normalization factor $c(k_2)$ equals $\sqrt{2}$ except if $k_2 = 0$ or $k_2 = 2\pi$, in which case this factor equals unity.

The physics of the + inter-ring states is that they are linear combinations of one-exciton Bloch states on two different rings of the cylinder. They have been constructed in such a way that they are eigenstates of the total Hamiltonian eq 1 with the energy

$$E_{\text{inter}}(\mathbf{K},\mathbf{k}) = 2\epsilon - 4J_1\cos(K_1/2)\cos(k_1/2) - 4J_2\cos(K_2/2)\cos(k_2/2) \quad (21)$$

if we neglect the coupling to the intra-ring states, i.e., if we impose an effective Pauli exclusion for double excitation of a single ring. This exclusion is clear from the factor $\sin|k_1(n_1 - m_1)/2|$ in eq 20. In fact, these states can be interpreted as the two-exciton eigenstates of an effective one-dimensional aggregate (with periodic boundary conditions) of N_1 effective two-level molecules, labeled by n_1 and m_1, with transition energies $\epsilon - 2J_2\cos(K_2/2)\cos(k_2/2)$ and excitation hopping rate $-J_1$. This analogy will be important in section VD.

The second type of inter-ring states, the "−" states, take the form

$$|\mathbf{K},\mathbf{k}\rangle_- = \frac{1}{N}\sum_{\mathbf{n},\mathbf{m}} \exp\left(i\mathbf{K}\cdot\frac{\mathbf{n}+\mathbf{m}}{2}\right) f_-(\mathbf{n}-\mathbf{m}) b_{\mathbf{n}}^{\dagger} b_{\mathbf{m}}^{\dagger}|g\rangle \quad (22)$$

with

$$f_-(\mathbf{n}-\mathbf{m}) = c(k_2)\,\sin\left(k_1\frac{n_1-m_1}{2}\right)\sin\left(k_2\frac{n_2-m_2}{2}\right) \quad (23)$$

Here the COM momentum $\mathbf{K}$ and the second component k_2 of the relative momentum are quantized according to the same rules as for the + states (except that $l_2' = 0$ and $l_2' = N_2$ are excluded). On the other hand, k_1 is quantized in a different way: $k_1 = 2\pi l_1'/N_1$, with $l_1' = 2, 4, ..., N_1 - 2$ if l_1 is even and $l_1' = 1, 3, ..., N_1 - 1$ if l_1 is odd (upper boundaries interchanged if N_1 is odd). This difference in quantization rules results from the fact that the periodic boundary conditions work out in a different way for the factor $\sin|k_1(n_1 - m_1)/2|$ in the + states than for the factor $\sin(k_1(n_1 - m_1)/2)$ in the − states (the absolute value in the former is necessary to guarantee that $f_+(\mathbf{n}-\mathbf{m}) = f_+(\mathbf{m}-\mathbf{n})$). The − states do not have the simple effective one-dimensional interpretation as the + states. However, under the imposed Pauli exclusion of double excitation of a single ring, they do represent eigenstates of the total Hamiltonian with the energy $E_{\text{inter}}(\mathbf{K},\mathbf{k})$.

The total set of states $|\mathbf{K},k_2\rangle$, $|\mathbf{K},\mathbf{k}\rangle_+$, and $|\mathbf{K},\mathbf{k}\rangle_-$ form a complete basis of two-exciton states on the cylinder (or on any two-dimensional manifold with periodic boundary conditions). They have been constructed such that they are "almost" eigenstates of the total Hamiltonian H in eq 1. We only neglected the matrix elements $\langle K',k_2'|H|\mathbf{K},\mathbf{k}\rangle_\pm$ which may mix the intra-ring states with the inter-ring ones. As H conserves momentum, these elements vanish if $\mathbf{K} \neq \mathbf{K}'$. In addition, it turns out that the − states do not couple to the intra-ring states due to their antisymmetric nature in the ring direction. We thus arrive at the following exact set of equations for the two-exciton states with COM momentum $\mathbf{K}$ on the cylinder:

$$H|\mathbf{K},\mathbf{k}\rangle_+ = E_{\text{inter}}(\mathbf{K},\mathbf{k})|\mathbf{K},\mathbf{k}\rangle_+ + \sum_{k_2'} c(\mathbf{K},\mathbf{k},k_2')|\mathbf{K},k_2'\rangle \quad (24)$$

$$H|\mathbf{K},k_2'\rangle = E_{\text{intra}}(\mathbf{K},k_2')|\mathbf{K},k_2'\rangle + \sum_{\mathbf{k}} c(\mathbf{K},\mathbf{k},k_2')|\mathbf{K},\mathbf{k}\rangle_+ \quad (25)$$

$$H|\mathbf{K},\mathbf{k}''\rangle_- = E_{\text{inter}}(\mathbf{K},\mathbf{k}'')|\mathbf{K},\mathbf{k}''\rangle_- \quad (26)$$

Here the coupling constant $c(\mathbf{K},\mathbf{k},k_2') = \langle \mathbf{K},k_2'|H|\mathbf{K},\mathbf{k}\rangle_+$ is given by

$$c(\mathbf{K},\mathbf{k},k_2') = -\frac{4J_1 c(k_2)}{N_2\sqrt{N_1}} \cos\frac{K_1}{2} \sin\frac{k_1}{2}\left[\cot\left(\frac{k_2+k_2'}{4}\right) - \cot\left(\frac{k_2-k_2'}{4}\right)\right] \quad (27)$$

We find that, naturally, the coupling is proportional to J_1. In addition, the couplings between the optically dominant states (those with small values of all wavenumbers involved, see below) can be seen to scale proportional to $1/N_1^{3/2}$. This size scaling arises from the fact that an inter-ring two-exciton state can only couple to an intra-ring one if the excitations are on neighboring rings. The probability for this is suppressed by the delocalization along the cylinder and even further due to the imposed Pauli exclusion for the inter-ring states.

We finally observe that in the case $K_1 = \pi$, the coupling constant $c(\mathbf{K},\mathbf{k},k_2')$ vanishes. This implies that for this special case, the basis states defined above are exact eigenstates, which are independent of the value of J_1. The same is true for the energies of these states (see eq 21). Therefore, the pump−probe spectrum in which two-exciton states with $K_1 = \pi$ are excited is basically of the same shape as the one for isolated ring aggregates. The same can also be concluded from the hard-core boson expression eq 9 with 12. This situation is relevant for the case of the HJ aggregate ($J_1 < 0$), if the pump−probe delay time is long enough to allow the one-exciton created by the pump pulse to relax into the $\mathbf{q} = (\pi, 0)$ state that lies at the bottom of the one-exciton band.

B. Transition Dipoles. We next consider the matrix elements of the cylinder's total dipole operator (cf. section II) between the one-exciton states $|\mathbf{q}\rangle$ and the basis states defined in section VA. The algebra involved in calculating these matrix elements is straightforward, and here we just quote the results. For the intra-ring two-exciton states, we have

$$\langle \mathbf{K},k_2|\hat{\vec{\mu}}|\mathbf{q}\rangle = \delta_{K_1,q_1}\frac{1}{N_2}\left(\cot\frac{K_2+k_2-2q_2}{4} - \cot\frac{K_2-k_2-2q_2}{4}\right)\vec{\mu}(K_2-q_2) \quad (28)$$

Here, $\vec{\mu}(K_2 - q_2) = \vec{\mu}_{(0,K_2-q_2)}/\sqrt{N_1}$, with $\vec{\mu}_{(0,K_2-q_2)}$ the transition dipole between the cylinder's ground state and the one-exciton state with wave vector $(0,K_2-q_2)$, whose components can be obtained from eqs 5−7.

Using the same notation, we arrive at

$${}_+\langle \mathbf{K},\mathbf{k}|\hat{\vec{\mu}}|\mathbf{q}\rangle = \delta_{K_1,q_1}\frac{c(k_2)\vec{\mu}(K_2-k_2)}{2\sqrt{N_1}}(\delta_{K_2-k_2,2q_2} + \delta_{K_2+k_2,2q_2}) \times \left(\cot\frac{K_1+k_1}{4} - \cot\frac{K_1-k_1}{4}\right) \quad (29)$$

and

$${}_-\langle \mathbf{K},\mathbf{k}|\hat{\vec{\mu}}|\mathbf{q}\rangle = \delta_{K_1,q_1}\delta_{k_1,q_1}\frac{c(k_2)\sqrt{N_1}\vec{\mu}(K_2-k_2)}{2}(\delta_{K_2-k_2,2q_2} - \delta_{K_2+k_2,2q_2}) \quad (30)$$

C. Explanation of Pump−Probe Spectrum for $J_1 = 0$. We will now use the above knowledge of the two-exciton states on the cylinder to understand the pump−probe spectra that were presented in section IV. As before, we will restrict ourselves to the situation where the cylinder resides in the $\mathbf{q} = \mathbf{0}$ one-exciton state just before the probe pulse arrives. Moreover, to keep the discussion as simple as possible, we will only consider the spectrum for probe polarization parallel to the cylinder axis. In this situation, we have a single negative peak in the spectrum, arising from bleaching and stimulated emission of the $\mathbf{q} = \mathbf{0}$ one-exciton state. This negative peak occurs at the one-exciton band edge energy $\epsilon - 2J_1 - 2J_2$ and has intensity (dipole squared) $2N\mu_{||}^2$, where the factor N arises from the superradiant nature of the transition and the factor of 2 is due to the fact that bleaching and stimulated emission overlap.

We are left with the question at what energies the induced absorption peaks will take place and what are the intensities of these peaks. We will first consider the simplest case of vanishing inter-ring interactions ($J_1 = 0$). Then the coupling strength $c(\mathbf{K},\mathbf{k},k_2')$ between the inter-ring and intra-ring states vanishes (see eq 27), implying that the basis of inter-ring and intra-ring states introduced above is in fact a basis of two-exciton eigenstates. Thus, the induced absorption transitions may take place between the $\mathbf{q} = \mathbf{0}$ state and each of the basis states. As light with polarization parallel to the cylinder axis cannot transfer momentum to the exciton system (also see eqs 28−30), we only need to consider the basis states with $\mathbf{K} = \mathbf{0}$. Moreover, we observe from eq 30 that for this polarization, none of the − inter-ring states is dipole-allowed ($k_1 = 0$ only gives a trivial − state), while of all the + states only those with $k_2 = 0$ are dipole allowed. For $J_1 = 0$, the transitions from the $\mathbf{q} = \mathbf{0}$ state to the latter are all degenerate at the energy $(2\epsilon - 4J_2) - (\epsilon - 2J_2) = \epsilon - 2J_2$, which is exactly the one-exciton band edge energy (at $J_1 = 0$). This is not surprising: for $J_1 = 0$, the inter-ring states are two noninteracting excitons, whose band edge energy is exactly twice the one-exciton band edge energy. The total intensity of these degenerate transitions is given by $2(N_1 - 1)N_2\mu_{||}^2$, which is of the usual superradiant nature in $N = N_1N_2$, except that $N_1 - 1$ occurs in stead of N_1, because for the inter-ring two-exciton states one of the rings is excluded from receiving the second excitation. We thus observe that for $J_1 = 0$, we have a net negative peak at the one-exciton band edge energy of strength $2N_2\mu_{||}^2$, arising from a strong cancellation between degenerate bleaching and induced absorption peaks. This is illustrated in Figure 6a, where the induced absorption due to the inter-ring two-exciton states is indicated as curve A, while the bleaching and stimulated emission is represented by curve B. The net negative peak C = A + B equals exactly the bleaching and stimulated emission peak of a single ring, as is appropriate in the case $J_1 = 0$.

Finally, we should consider the induced absorption to the intra-ring two-exciton states. By definition, these states have the energies of the single-ring two-exciton states (independent of J_1). As for $J_1 = 0$, the energy of the $\mathbf{q} = \mathbf{0}$ one-exciton state also equals the energy $\epsilon - 2J_2$ of the optically allowed one-exciton state in a single ring; we thus find that the induced absorption peaks due to the intra-ring two-exciton states occur at the same positions as those for a single ring. Moreover, the dipoles of these transitions (eq 28) equal those for the single ring (none of these transitions is superradiant in the length N_1 of the cylinder). Thus, the induced absorption spectrum due to the intra-ring two-exciton states is identical to the induced absorption spectrum of a single ring. In particular, the dominant intra-ring induced absorption peak (curve D in Figure 6a) is due to the state $|\mathbf{K}=\mathbf{0},k_2=2\pi/N_2\rangle$, which occurs at the energy $2\epsilon - 4J_2\cos(\pi/N_2) = 2\epsilon - 4J_2 + \Delta_\perp$ (with $\Delta_\perp$ as defined in eq 14) and with intensity $4\mu_{||}^2\cot^2(\pi/(2N_2))/N_2 \approx 16N_2\mu_{||}^2/\pi^2$.

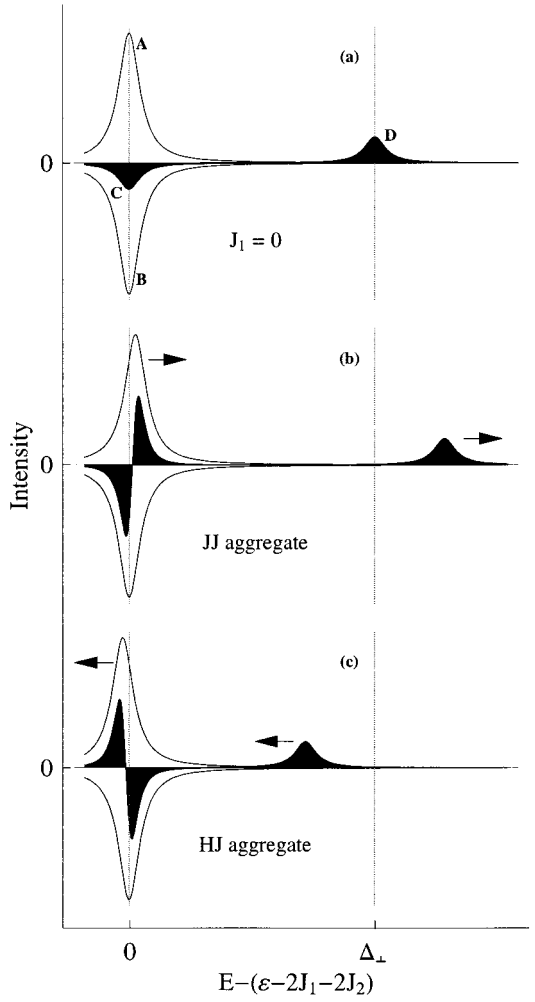

Figure 6. Schematic representation of how the total pump−probe spectrum of a cylinder results from the separate bleaching, stimulated emission, and induced absorption features. Panel a represents the case of vanishing inter-ring interactions ($J_1 = 0$), where the induced absorption due to inter-ring two-exciton states (curve A) is exactly resonant with the bleaching and stimulated emission of the $|\mathbf{q} = \mathbf{0}\rangle$ one-exciton state (curve B), resulting in a small net negative peak (curve C), which is in fact the bleaching and stimulated emission of a single ring. The intra-ring induced absorption peak (curve D) is blue-shifted relative to the bleaching over an amount $\Delta_\perp$. Both peaks in the net spectrum (shaded) have intensity proportional to N_2 and independent of N_1. Panel b represents the case of the JJ aggregate with finite J_1 (>0), in which case the one-exciton to inter-ring two-exciton-induced absorption peak is blue-shifted relative to the one-exciton bleaching and stimulated emission over $\Delta_{||}$, resulting in a net dispersive feature near the exciton band edge. The dispersive feature has peak intensities that scale like N_1N_2 (or $N_{coh}N_2$ in the case of a finite coherence length) and are much stronger than the intra-ring induced absorption feature ($\sim N_2$) that still exists and that shifts away from the bleaching peak with increasing J_1. The mixing between the inter-ring and intra-ring two-exciton states may be neglected over a large range of parameters (see text). The latter is not true for the HJ aggregate ($J_1 < 0$, panel c), where the intra-ring peak shifts closer to the inter-ring peak (part of the H-like dispersive feature) and quickly leads to mixing of these two types of states for increasing $|J_1|$.

Summarizing the above, we find that for the case $J_1 = 0$, the pump−probe spectrum of the cylinder properly reduces to the spectrum of a single ring, with an induced absorption peak of intensity $\sim N_2$ that is blue-shifted relative to the negative bleaching and stimulated emission peak by the Pauli exclusion gap $\Delta_\perp$. The negative peak results from a strong cancellation between exactly resonant induced absorption and bleaching/stimulated emission contributions.

D. Explanation of Pump−Probe Spectrum for $J_1 \neq 0$. Though the foregoing may be considered a complicated way to construct the pump−probe spectrum in the limit $J_1 = 0$, where we know a priori that the spectrum should reduce to the single-ring one, this construction turns out to be most useful to understand the changes that occur if we allow for finite values of J_1. In this case, again we consider the three basic contributions to the spectrum: (i) bleaching and stimulated emission of the $\mathbf{q} = \mathbf{0}$ state, (ii) induced absorption to the inter-ring two-exciton states, and (iii) induced absorption to the intra-ring two-exciton states.

For finite J_1, the peak due to bleaching and stimulated emission is still positioned at the one-exciton band edge, which now lies at $E = \epsilon - 2J_1 - 2J_2$. This explains the observed shift over $-2J_1$ of the bleaching peak in Figures 3 and 5 upon switching on J_1. In all cases, the negative peak has the superradiant intensity $2N\mu_{||}^2$. The inter-ring two exciton states that are optically allowed from the $\mathbf{q} = \mathbf{0}$ state still have the same quantum numbers as for the $J_1 = 0$ case. Specifically, only the + states $|\mathbf{K}=\mathbf{0},\mathbf{k}=(k_1,0)\rangle_+$ can contribute to the induced absorption. The finite value of J_1 has two consequences: (i) It lifts the mutual degeneracy of these states, as well as their degeneracy with twice the one-exciton band edge energy. (ii) It mixes these states with the intra-band states, through the coupling eq 27. As the former effect is most important (due to the degeneracy), we will first neglect the second effect and consider the states with lifted degeneracies as proper eigenstates. We will discuss the validity of this decoupling approximation at the end of this section.

The inter-ring state with the largest oscillator strength to the $\mathbf{q} = \mathbf{0}$ one-exciton is $|\mathbf{K}=\mathbf{0},\mathbf{k}=(2\pi/N_1,0)\rangle_+$. This state gives a positive contribution of intensity $16N\mu_{||}^2/\pi^2$ (from eq 29, assuming $N_1 \gg 1$) at $E = \epsilon - 2J_2 - 2J_1 + \Delta_{||}$, i.e., shifted relative to the bleaching feature by the effective Pauli gap $\Delta_{||}$ defined in eq 15. The important observation is that the new induced absorption peak that arises on the blue side (red side) of the bleaching peak for the JJ aggregate (HJ aggregate) in Figures 3 and 4 (Figure 5) upon switching on the inter-ring interaction J_1, results from the fact that the inter-ring induced absorption peaks, which were exactly resonant with the bleaching peak at $J_1 = 0$, are shifted away from this resonance at finite values of J_1. This shift, caused by the delocalization of the inter-ring one- and two-exciton states in the longitudinal direction of the cylinder, means that these contributions no longer add to a single peak of small intensity ($\sim N_2$) but, rather, form a dispersive feature, reminiscent of a one-dimensional J aggregate (H aggregate), as is seen in Figure 3 (Figure 5). This is schematically depicted in Figure 6b for the JJ aggregate and Figure 6c for the HJ aggregate. This effective one-dimensional behavior is a direct consequence of the fact that the + inter-ring two-exciton states behave like the two-exciton states on an effective one-dimensional aggregate of length N_1, as was noted below eq 21.

The shift over $\Delta_{||}$ is most clearly seen in Figure 4, where we used very small line widths η. Here we also observe the large intensities ($\sim N\mu_{||}^2$) of both separate contributions relative to the net bleaching intensity $2N_2\mu_{||}^2$ in the case $J_1 = 0$. These large intensities arise from the superradiant nature of both transitions involved, caused by the complete coherence of the relevant one- and two-exciton states over the cylinder.

We are left to determine the induced absorption contributions due to the intra-ring two-exciton states. The dominant one of these states is $|\mathbf{K}=\mathbf{0},k_2=2\pi/N_2\rangle$, which is responsible for a positive ("single-ring") peak of intensity $16N_2\mu_{||}^2/\pi^2$ (from eq

28) at the position $E = \epsilon - 2J_2 + 2J_1 + \Delta_\perp$, i.e., shifted relative to the bleaching peak by $4J_1 + \Delta_\perp$. This explains why the single-ring peak which exists for $J_1 = 0$ is seen to shift away from the bleaching peak when switching on J_1 for the JJ aggregate (Figures 3 and 4), while it shifts toward the bleaching peak for the HJ aggregate (Figure 5). This is also schematically depicted in Figure 6. We finally observe that the intra-ring induced absorption peak keeps a constant intensity ($\sim N_2$), which explains why upon switching on J_1, it rapidly becomes invisible relative to the band edge feature, which has intensity $\sim N_1 N_2$, as we have seen above.

As noted already, the above phenomena are most clearly observed in Figure 4, where the line width η is small, allowing for all inter-ring two-exciton states to be resolved. In Figures 3 and 5, this is not the case, and the situation is slightly more complicated because we used a line width that is large enough to limit the coherence length N_{coh} (eq 13) of the excitons along the cylinder to a number smaller than or comparable to the cylinder length N_1. In this case, the different inter-ring induced absorption peaks merge into one peak which for the JJ aggregate is blue shifted by an amount $\sim\eta$ compared to the bleaching peak, while for the HJ aggregate, it is red-shifted,[37] and the intensities of the bleaching and induced absorption peaks are both $\sim N_{\mathrm{coh}} N_2 \mu_{\|}^2$. The coherence of the excitons along the circumference of a ring is still always guaranteed at the η values we used.

The above arguments, based on completely decoupled inter-ring and intra-ring two-exciton states, explain with surprising success the details of the spectra for the JJ aggregate in Figures 3 and 4. In particular, the detuning within the dispersive feature and the growth of the intensity of the dispersive feature relative to the intra-ring peak for the JJ aggregate are understood well from the above. In addition, the fine structure that emerges in the dispersive feature in Figure 3g,h indicates that the coherence length gets in the order of the cylinder length.

To understand the success of the decoupling approximation for the JJ aggregate, we have to compare the coupling between the dominant inter-ring and intra-ring states to the detuning Δ between them. The former is given by $c(\mathbf{K}=\mathbf{0},\mathbf{k}=(2\pi/N_1,0), k_2'=2\pi/N_2) \approx -16J_1/N_1^{3/2}$ while the latter reads:

$$\Delta = 4J_1 + \Delta_\perp - \Delta_{\|} \approx 4J_1 + \frac{2\pi^2 J_2}{N_2^2} \qquad (31)$$

where in the last step we have assumed that $N_1 \gg 1$ and $N_2 \gg 1$. As we see, for the JJ aggregate, both the coupling and the detuning increase linearly in J_1, where in fact the detuning increases much faster ($N_1^{3/2} \gg 4$). Thus, it appears that neglecting the coupling between the intra-ring and inter-ring states is always justified for the JJ aggregate and that for increasing J_1 the pump−probe spectrum of the cylinder will look more and more like the spectrum of an effective ring of length N_1, deriving from the inter-ring two-exciton states. This explains why all details of the spectra for all values of J_1 in Figures 3 and 4 can be understood even at a quantitative level within the decoupling approximation. It should be realized, however, that still there is a limit to the validity of the approximation. If J_1 is large compared to J_2, all $N_2/2$ intra-ring two-exciton states $|\mathbf{K}=\mathbf{0},k_2\rangle$ are equally close (on the scale of $4J_1$) to the dominant inter-ring state. Thus, as a crude estimate, the coupling of the latter to the intra-ring subspace then becomes of the order $8N_2J_1/N_1^{3/2}$. Comparing this to the detuning $4J_1$, we observe that the approximation necessarily breaks down when N_2 is comparable to or larger than N_1 (and at the same time $J_1 \gg J_2$).

The above estimates also explain why the spectra for the HJ aggregate (Figure 5) with increasing value of $|J_1|$ in general do not approach the simple situation where they can be interpreted as deriving solely from the inter-ring two-exciton states (which would yield a one-dimensional H aggregate spectrum). The reason is that then with increasing $|J_1|$, the detuning Δ defined by eq 31 decreases so that the approximation deteriorates.

VI. Conclusions

In this paper, we have studied the optical response of cylindrical molecular aggregates consisting of stacked rings. We have seen that the linear absorption spectrum of these aggregates exhibits two peaks with mutually perpendicular polarization. This is not due to a Davydov splitting but, rather, is a purely geometric effect, caused by the optical selection rules that make three optical transitions dipole allowed (two of which are degenerate). The splitting between both peaks is set by the circumference N_2 of the cylinder and the excitation transfer interaction between the molecules in the circumferential direction. This allows one to obtain information on N_2 from absorption experiments, as has indeed been done in ref 17.

Most attention in this paper has been devoted to the pump−probe (or transient absorption) spectrum, where we have limited ourselves to the case where the cylinder resides in the $|\mathbf{q} = \mathbf{0}\rangle$ one-exciton state when the probe pulse arrives. We have seen strong changes of the pump−probe spectrum when switching on the inter-ring interactions J_1. In particular, we have seen that the frequency scale characterizing the spectral features changes from the single-ring Pauli exclusion gap ($\Delta_\perp$) for $J_1 = 0$ to the generally much smaller Pauli exclusion gap ($\Delta_{\|}$) for effective two-level systems on a ring of circumference N_1 and interaction J_1. These changes can be understood from a separation of the two-exciton states into those with both excitations in different rings of the cylinder and those with the two excitations within the same ring. Figure 6 gives a pictorial presentation of this explanation. The separation into inter-ring and intra-ring two-exciton states holds over a wide range of parameter values in the case of the JJ aggregate, while it has a much more limited validity in the case of HJ aggregates (see end of section V).

As one of the key results, our analysis shows that for the JJ aggregate, over a large range of system parameters, the pump−probe spectrum of the cylinder is simply equivalent to the spectrum for an effective one-dimensional ring-shaped J aggregate with length N_1, effective molecular frequency $\epsilon - 2J_2$ (at $\mathbf{K} = \mathbf{0}$), and intermolecular interaction $-J_1$. As the one-dimensional case has been well-studied, this is very useful when analyzing experiments. In particular, this tells us that the detuning Δ_{pp} between the positive and negative peaks within the dispersive feature near the exciton band edge is either determined by the length N_1 of the cylinder or by the coherence length N_{coh} if the latter is smaller than N_1. In the current paper, this coherence length is set by the homogeneous line width η, cf. eq 13. More generally, this length is also limited by scattering on static disorder (random molecular transition energies and intermolecular interactions). Though we did not include such disorder, the knowledge of one-dimensional systems[26] does allow us to conclude that the detuning Δ_{pp} then gives the delocalization length of the excitons in the direction of the cylinder through the expression $N_{\mathrm{del}} \approx (2\pi^2 J_1/\Delta_{\mathrm{pp}})^{1/2}$. This expression, which involves knowledge of J_1, only holds if static disorder dominates the scattering of the excitons. Yet at the

same time, the disorder strength should be weak compared to $\Delta_\perp$, as otherwise the disorder will lead to localization of the exciton states in the circumferential direction as well so that the entire picture of intra-ring and inter-ring two-exciton states will break down.

We note that the above also applies to some extent to the HJ aggregate, where a dispersive feature characteristic of a one-dimensional H aggregate arises near the exciton band-edge upon switching on J_1. However, as we have seen (cf. Figure 5), this feature generally does not dominate the intra-ring induced absorption peak and, moreover, only exists as an isolated spectral feature for a small range of parameter values.

We finally address the connection to experiment. In section II, we have already mentioned that the linear absorption spectrum of TDBC/C8O3 aggregates indeed exhibits a double-peak structure near 600 nm,[17] with a peak separation of ~30 nm ~830 cm^{-1}, which (assuming J_1 to be negligible) has been translated into a cylinder circumference of $N_2 = 7.3$ (i.e., 7 or 8) molecules. From the intensity ratio of the two absorption bands, the angle β was found to lie in the range 20−32°. The fairly large uncertainty in this angle stems from some arbitrariness in fitting the absorption bands. The same aggregates have also been studied in pump−probe experiments. Like we assumed throughout this paper, the aggregates were pumped in the lowest, i.e., $\mathbf{q} = \mathbf{0}$, absorption band. The observed spectrum indeed has the dispersive shape characteristic for one-dimensional J aggregates (induced absorption blue-shifted relative to the bleaching) with a blue shift $\Delta_{pp} \approx 1.2$ nm ~33 cm^{-1} at $T = 1.5$ K.[42] The blue shift suggests that we are dealing with JJ aggregates, which seems surprising, as the above values for β fall outside the interval $35.3° < \beta < 54.7°$ that gives a JJ aggregate (section IV). One should keep in mind, however, that this interval was determined assuming only nearest-neighbor interactions ($-J_1$ and $-J_2$). On a two-dimensional manifold, like the cylinder, this certainly is a crude approximation. It is interesting, however, that all expressions derived for the $\mathbf{K} = \mathbf{0}$ two-exciton states in section V remain valid if we include in addition the interactions $J_r \equiv -J(\mathbf{m}=(1,1))$ and $J_{/} \equiv -J(\mathbf{m}=(1,-1))$. These represent the interactions in the right-handed and left-handed diagonal direction of the lattice, respectively. The only effect of these interactions, is that in section V we should replace J_1 by an effective inter-ring interaction $\tilde{J}_1 \equiv J_1 + J_r + J_{/}$. Straightforward algebra shows that, assuming point-dipole interactions, $\tilde{J}_1$ may be negative over a larger range of angles β than J_1. The details of this behavior depend on the ratio of lattice constants. As an example, we consider a square lattice and an angle $\beta = 32°$ (i.e., the largest angle consistent with experiment). We then indeed find a JJ aggregate with $\tilde{J}_1 = 0.17J_2$. The finite values for J_1, J_r, and $J_{/}$ lead to a slight increase of the circumference, as determined from the linear absorption spectrum, to $N_2 = 7.8$ molecules. On the other hand, the value for $\tilde{J}_1$ allows us to estimate $N_{del} \approx 10$ from the observed value for the blue shift, Δ_{pp}, in the pump−probe spectrum. This gives a total value of $N_{del} \times N_2 \approx 80$ for the number of molecules in the cylinder participating in the excitation (the delocalization area). This number is rough, as detailed information on the arrangement of the molecules in the cylinders is lacking at the moment. A further discussion of the experimental pump−probe spectra, in particular of the influence of varying the temperature and the pump frequency within the lowest exciton band, will be given in ref 42.

Acknowledgment. We thank Dr. G. Juzeliūnas, Prof. Dr. S. Daehne, Prof. Dr. K. Duppen, and Dr. S. Lampoura for many stimulating discussions. M.B. gratefully acknowledges Nuffic for financial support through a Huygens Fellowship. This work is part of the research programs of the Stichting voor Fundamenteel Onderzoek der Materie (FOM) and INTAS (Project 97-10434).

References and Notes

(1) Jelley, E. E. *Nature* **1937**, *139*, 631.
(2) Scheibe, G. *Angew. Chem.* **1937**, *50*, 212.
(3) In *J-Aggregates*; Kobayashi T., Ed.; World Scientific: Singapore, 1996.
(4) Kirstein, S.; Möhwald, H.; Shimomura, M. *Chem Phys. Lett.* **1989**, *154*, 303.
(5) Nabetani, A.; Tomioka, A.; Tamaru, H.; Miyano, K. *J. Chem. Phys.* **1995**, *102*, 5109.
(6) Ecoffet, C.; Markovitsi, D.; Millié, P.; Lemaistre, J. P. *Chem. Phys.* **1993**, *177*, 629.
(7) Markovitsi, D.; Germain, A.; Millié, P.; Lécuyer, P.; Gallos, L.; Argyrakis, P.; Bengs, H.; Ringsdorf, H. *J. Phys. Chem.* **1995**, *99*, 1005.
(8) Spano, F. C. *J. Chem. Phys.* **2001**, *114*, 5376.
(9) McDermott, G.; Prince, S. M.; Freer, A. A.; HawthornthwaiteLawless, A. M.; Papiz, M. Z.; Cogdell, R. J.; Isaacs, N. W. *Nature* **1995**, *374*, 517.
(10) Koepke, J.; Hu, X.; Muenke, C.; Schulten, K.; Michel, H. *Structure* **1996**, *4*, 581.
(11) See, e.g.: van Amerongen, H.; Valkunas, L.; van Grondelle, R. *Photosynthetic Excitons*; World Scientific: Singapore, 2000.
(12) Nozawa, T.; Ohtomo, K.; Suzuki, M.; Morishita, Y.; Madigan, M. *Bull. Chem. Soc. Jpn.* **1993**, *66*, 231.
(13) Novoderezhkin, V. I.; Fetisova, Z. G. *Biochem. Mol. Biol. Int.* **1996**, *40*, 243.
(14) Prokhorenko, V. I.; Steensgaard, D. B.; Holzwarth, A. R. *Biophys. J.* **2000** *79*, 2105.
(15) Pawlik, A.; Kirstein, S.; De Rossi, U.; Daehne, S. *J. Phys. Chem. B* **1997**, *101*, 5646.
(16) Kirstein, S.; von Berlepsch, H.; Böttcher, C.; Burger, C.; Ouart, A.; Reck, G.; Daehne, S. *Chem. Phys. Chem.* **2000**, *3*, 146.
(17) Spitz, C.; Knoester, J.; Ouart, A.; Daehne, S. *Chem. Phys.*, in press.
(18) Malyshev, V.; Moreno, P. *Phys. Rev. B* **1995**, *51*, 14587.
(19) Bakalis, L. D.; Knoester, J. *J. Lumin.* **2000** *87*−*89*, 66.
(20) Gadonas, R.; Danielus, R.; Piskarskas, R.; Rentsch, S. *Izv. Akad. Nauk SSSR, Ser. Fiz.* **1983**, *47*, 2445 [*Bull. Acad. Sci. USSR, Phys. Ser.* **1983**, *47*, 151].
(21) Fidder, H.; Knoester, J.; Wiersma, D. A. *J. Chem. Phys.* **1993**, *98*, 6564.
(22) Johnson, A. E.; Kumazaki, S.; Yoshihara, K. *Chem Phys. Lett.* **1993**, *211*, 511.
(23) Minoshima, K.; Taiji, M.; Misawa, K.; Kobayashi, T. *Chem. Phys. Lett.* **1994**, *218*, 67.
(24) Juzeliūnas, G. *Z. Phys. D* **1988**, *8*, 379.
(25) Meier, T.; Chernyak, V.; Mukamel, S. *J. Phys. Chem. B* **1997**, *101*, 7332.
(26) Bakalis, L. D.; Knoester, J. *J. Phys. Chem. B* **1999**, *103*, 6620.
(27) Davydov, A. S. *Theory of Molecular Excitons*; Plenum: New York, 1971.
(28) Agranovich, V. M.; Galanin, M. D. In *Electronic Excitation Energy Transfer in Condensed Matter*; Agranovich, V. M., Maradudin, A. A., Eds.; North-Holland: Amsterdam, 1982.
(29) Bakalis, L. D.; Knoester, J. *J. Chem. Phys.* **1997**, *106*, 6964.
(30) Agranovich, V. M.; Basko, D. M. *J. Chem. Phys.* **2000**, *112*, 8156.
(31) Didraga, C.; Knoester, J. *Chem. Phys.*, in press.
(32) Mukamel, S. *Principles of Nonlinear Optical Spectroscopy*; Oxford: Oxford, 1995.
(33) Leegwater, J. A.; Mukamel, S. *Phys. Rev. A* **1992**, *46*, 452.
(34) Juzeliūnas, G.; Knoester, J. *J. Chem. Phys.* **2000**, *112*, 2325.
(35) Montroll, E. *J. Math. Phys.* **1969**, *10*, 752.
(36) Juzeliūnas, G.; Reineker, P. *J. Chem. Phys.* **1998**, *109*, 6916.
(37) Spano, F. C. *Nonlinear Optics* **1995**, *12*, 275.
(38) Ishihara, H.; Cho, K. *Phys. Rev. B* **1990**, *42*, 1724.
(39) Spano, F. C. *J. Chem. Phys.* **1992**, *96*, 8109.
(40) Novoderezhkin, V. I.; Razjivin, A. P. *FEBS* **1993**, *330*, 5.
(41) Knoester, J.; Spano, F. C. In ref 3, p 111.
(42) Lampoura, S.; Spitz, C.; Daehne, S.; Knoester, J.; Duppen, K. *J. Phys. Chem. B*, submitted.